Florida State University Libraries

2020

An Estimation of the Production of pp → Zγγ Events at √s = 13 TeV Using the CMS Detector

Michael Louis Campanella

THE FLORIDA STATE UNIVERSITY

COLLEGE OF ARTS & SCIENCES

AN ESTIMATION OF THE PRODUCTION OF $pp \to Z\gamma\gamma$ EVENTS AT

$\sqrt{s} = 13$ TeV USING THE CMS DETECTOR

BY

MICHAEL CAMPANELLA

A Thesis submitted to the
Department of Physics
in partial fulfillment of the requirements for graduation with
Honors in the Major

Degree Awarded:
Spring, 2020

The members of the Defense Committee approve the thesis of Michael
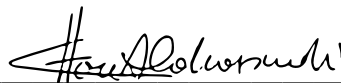Campanella defended on April 13, 2020

_____
Dr. Andrew Askew
Thesis Director

_____
Dr. Rachel Yohay
Committee Member

_____
Dr. Ettore Aldrovandi
Outside Committee Member

2

Abstract

This thesis estimates the production of $pp \to Z\gamma\gamma$ events where the Z boson decays to two muons. This analysis will use the data from Run 2 of the CMS detector. For Run 2, CMS collided protons at $\sqrt{s} = 13$ TeV and had an integrated luminosity of 136.1 fb^{-1}. This is the first analysis to examine this final state at $\sqrt{s} = 13$ TeV. It is also the first analysis to estimate the background using an entirely data based method. 1024.25 ± 61.18 events in this final state were observed. The estimated number of background events was 1301.75 ± 133.85. The Standard Model prediction is 681.86 ± 148.17 events, so there was an excess in the observed number of signal events over the Standard Model prediction.

Contents

List of Figures

List of Tables

1 Introduction

The Standard Model of particle physics (SM) describes the fundamental particles and their interactions. These elementary particles are divided into two categories: fermions and bosons. All matter is comprised of fermions, whereas vector bosons are force mediators. Fermions are further divided into quarks and leptons. Quarks can have a charge of $+\frac{2}{3}e$ or $-\frac{1}{3}e$ where e is the fundamental charge. Quarks bind together to make hadrons, like protons. The other fundamental particles that are important for this analysis are muons, photons, and Z bosons. Muons are second generation leptons. Muons have a charge of $-e$ and a rest mass of approximately 105 MeV. Photons are massless, vector bosons with no charge. They mediate electromagnetic interactions. Z bosons are vector bosons that mediate the weak interaction. Z bosons have no charge, but they have a rest mass of about 91 GeV. Z bosons have a very short lifetime of approximately 3 x 10^{-25} s [1].

The SM can be used to calculate the probability that a particular interaction will occur during a particle collision. To test the SM, this prediction is compared to the experimental results, which is what will be done in this analysis.

This analysis will focus on the process $pp \rightarrow Z\gamma\gamma$. The Z boson almost immediately decays into either neutrinos, electrons, muons, taus, or hadrons. Hadrons are the most likely decay product. However, the final

state that will be considered in this analysis is $\mu\mu\gamma\gamma$ because the muon channel has lower background. The SM allows three interactions at leading order that produce this final state from a pp collision. The first interaction involves initial state radiation (ISR). ISR occurs when photons radiate off of the incident quarks before the collision (Figure 1a). The second interaction involves final state radiation (FSR). FSR occurs when photons radiate off of the final state leptons after the collision (Figure 1b). The third interaction is a combination of ISR and FSR (Figure 1c).
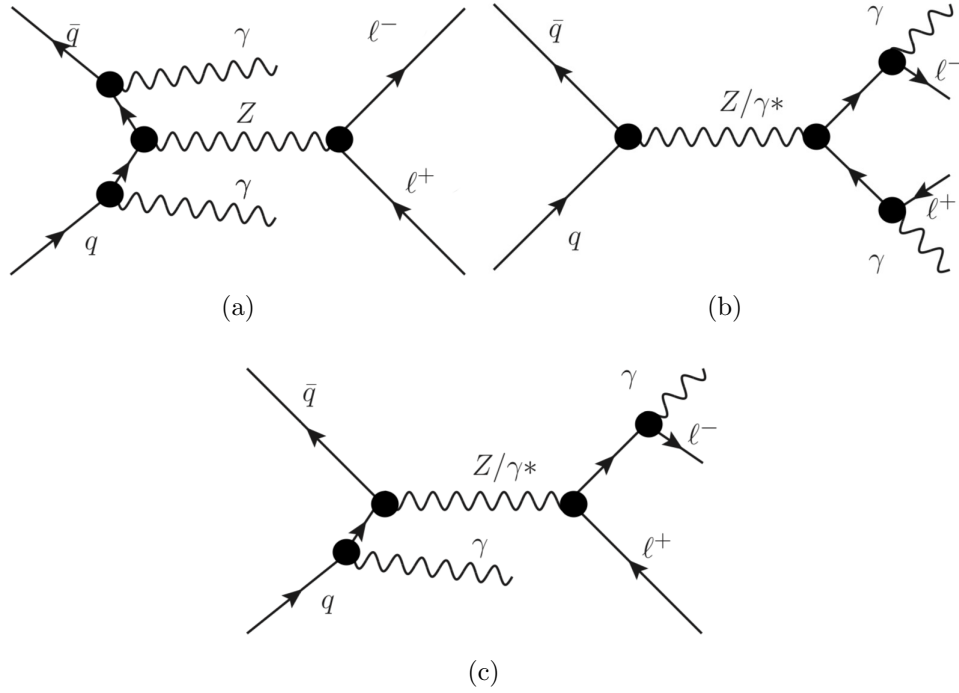
Figure 1: The Standard Model leading order diagrams for $Z\gamma\gamma$ production. Figure 1a depicts the case where the photons originate from initial state radiation, Figure 1b where the photons originate from final state radiation, and Figure 1c where the photons could originate from either.

A statistically significant excess in this final state over the Standard Model prediction could be evidence of new physics. One possibility is anomalous quartic gauge-boson couplings. The quartic gauge-boson couplings $ZZ\gamma\gamma$ and $Z\gamma\gamma\gamma$ (Figure 2) are forbidden in the Standard Model [2]. Evidence for such an interaction could be indicative of new physics.
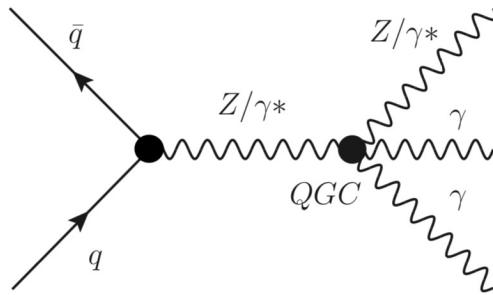
Figure 2: Feynman diagram of an anomalous quartic gauge-boson coupling which is forbidden in the Standard Model.

The main source of background for this analysis is jets misidentified as photons. A jet is a cone of hadrons. Jets are formed when a parton from the interaction hadronizes to create a collimated set of particles. Jets have a large cross section for pp collisions. This is the first analysis to estimate the background for this interaction using an entirely data-based method.

This analysis will estimate the number of $Z\gamma\gamma$ events where the Z boson subsequently decays to two muons produced during proton - proton collisions with $\sqrt{s} = 13$ TeV at the Compact Muon Solenoid (CMS) detector. The entirety of the Run 2 data, which had an integrated luminosity of 136.1 fb^{-1}, will be used in this analysis. This process has not yet been observed at $\sqrt{s} = 13$ TeV.

11

2 The CMS Detector

The Large Hadron Collider (LHC) is a pp collider located along the border between France and Switzerland. The geometry of the CMS detector is a cylindrical where the beam line is along the longitudinal axis. p_T or transverse momentum is defined as the momentum of a particle orthogonal to the beam-line. The azimuthal angle is denoted as ϕ. Instead of using the polar angle, it is convenient to use the pseudo-rapidity, η, which is the angle with respect to the axis of the colliding beams (Figure 3). Pseudo-rapidity is defined as:

$$\eta = -\log \tan\left(\frac{\theta}{2}\right) \tag{1}$$

where θ is the polar angle.
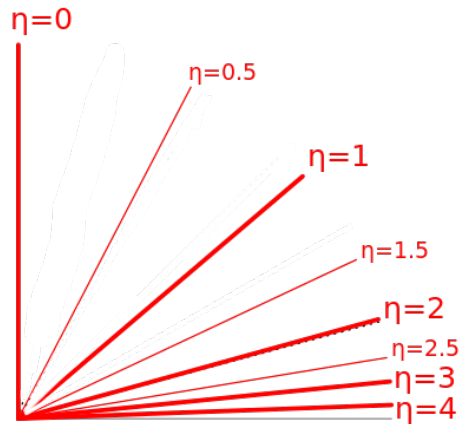
Figure 3: Several pseudo-rapidities where the beamline is along the x - axis and $\eta = 0$ is above the collision.

12

Angular separation between objects is denoted as ΔR and is defined as:

$$\Delta R = \sqrt{\Delta\phi^2 + \Delta\eta^2} \tag{2}$$

The CMS detector is composed of a four Tesla solenoid and four subdetectors: the tracker, the electromagnetic calorimeter (ECAL), the hadronic calorimeter (HCAL), and the muon system (Figure 4). This analysis will be performed using the data from all the parts of the detector.
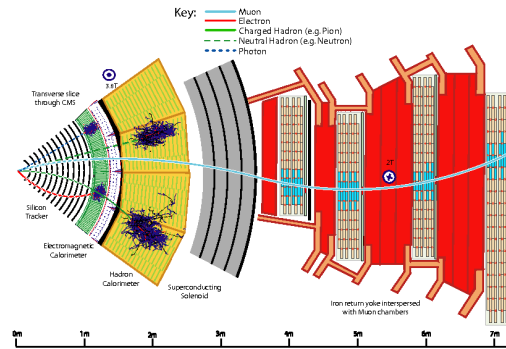
Figure 4: A portion of the cross section of the CMS detector.

The tracker is made entirely out of silicon, and it records the path of charged particles by recording their position at a number of points [3]. Since the particles are traveling through a magnetic field, their path is curved. The radius of curvature can be used to calculate the transverse momentum of the particle.

The ECAL is a homogeneous calorimeter composed of lead tungstate crystals. When a electromagnetic particle enters the ECAL, it interacts

with the crystal creating an electromangetic shower. An electromagnetic shower is composed of photons, electrons, and positrons. The processes that are responsible for EM showers are the pair-production of the photons and the bremsstrahlung of the electrons and positrons. The shower then ionizes the crystal producing scintillation light. This light is recorded and is proportional to the incident particle's energy. The ECAL primarily measures the energies of electromagnetic particles like photons and electrons [4]. The ECAL will be used in this analysis to identify photon candidates.

The HCAL is a sampling calorimeter, and it is composed of alternating layers of brass absorbers and plastic scintillator. When a hadron interacts with the absorber, it produces a hadronic shower. A hadronic shower can be composed of neutral and charged hadrons, as well as leptons and photons. There are many different nuclear processes that occur during a hadronic shower, thus they are more difficult to characterize than electromagnetic showers. Hadronic showers also have different shapes than electromagnetic showers. The particles of the hadronic shower then interact with the scintillator producing light. The amount of light in the HCAL tower is proportional to the energy of the incident hadron [5].

The muon system is composed of four muon stations. The path of the particle is determined by tracking its position as it travels through the muon stations. Combining the data from the muon system and the tracker yields the complete path of the particle. Since there is so much material between the beamline and the muon system, typically muons are the only

charged particle that can reach the system. Muons can reach the system because muons are minimum ionizing particles and because muons have relatively long lifetimes since they are in boosted frames and decay weakly. The muon system will be used to identify muon candidates in the analysis [6].

3 Event Selection

3.1 Selection Quantities

The first quantity that will be used is isolation. Cuts are made on isolation in order to to discriminate against high energy objects. Three types of isolations are used in this analysis. The first type of isolation is photon isolation. Photon Isolation (PhoIso) is defined as the amount of energy deposited by other electromagnetic objects in the ECAL in a cone of $\Delta R < .3$ in the direction of the electromangetic object. The second type of isolation is Neutral Hadron Isolation. Neutral Hadron Isolation (NeuIso) is defined as the amount of energy deposited by neutral hadrons, i.e. energy in the HCAL that does not have an associated track in the tracker, in a cone of $\Delta R < .3$ in the direction of the electromagnetic object. The third type of isolation is Charged Hadron Isolation. Charged Hadron Isolation (CHIso) is defined as the amount of energy deposited by charged hadrons, i.e. energy in the HCAL that has an associated track in the tracker, in a cone of $\Delta R < .3$ in the direction of the electromagnetic object.

Another quantity that is used in selecting photons is H/E. H/E is the ratio of energy deposited in the HCAL tower behind the seed crystal in the ECAL over the energy deposited in the supercluster in the ECAL. H/E is used to distinguish between photons and hadronic events that underwent an early conversion in the elctromagnetic calorimeter.

The final quantity that is used is $\sigma_{i\eta i\eta}$. $\sigma_{i\eta i\eta}$ is a shower shape mea-

surement. It is the square root of the variance of the events energy distribution in the ECAL in η about the mean. Photons have a well defined shower shape, so cuts on $\sigma_{i\eta i\eta}$ discriminate against jets.

3.2   Selection

The final state that is of interest for this analysis is $\mu\mu\gamma\gamma$. Selection requirements are made on the events in order to enrich the sample with the final state. For this analysis, events are selected using the dimuon trigger. Then, it was required that each event additionally had two photon candidates with $p_T > 10$ GeV with no other quality requirements made. The candidate events must pass the following additional selection requirements:

- Both muons must pass medium muon selection requirements.

- Both muons must have $p_T > 25$ GeV.

- Muons are required to be separated by $\Delta R > .3$.

- The event is required to have two electromagnetic (EM) objects that pass loose photon selection requirements.

- EM objects are required to be separated from each other and the muons by $\Delta R > .\ 6$.

Loose photon selection requirements are the following.
For the barrel:

17

- $p_T > 15$ GeV,

- H/E < .105,

- NeuIso < $9.188 + .0126 * p_T + .000026 * p_T^2$,

- PhoIso < $2.956 + .0035 * p_T$,

- CHIso < 2.839 ,

- $\sigma_{i\eta i\eta} < .0103$.

For the Endcap:

- $p_T > 15$ GeV,

- H/E < .029,

- NeuIso < $10.471 + .0119 * p_T + .000025 * p_T^2$,

- PhoIso < $4.895 + .004 * p_T$,

- CHIso < 2.150 ,

- $\sigma_{i\eta i\eta} < .0276$.

The cuts are applied in succession leading to 2920 candidate events (Table 1).

Requirement Applied	Number of Events
Events Selected by Dimuon Trigger that also have two photon candidates	36196700
Two Medium Muons	24049440
Muon $p_T > 25$ GeV	1367730
One Loose Photon	123193
Two Loose Photons	5444
Separation requirements and Requiring photons to be in barrel or endcap	2326

Table 1: The number of events remaining after each cut is applied.

4   Background Estimation

In order to estimate the number of background events, the fake ratio must be estimated. The fake ratio (f) is the ratio of jet candidates that pass certain selection requirements over the number of jets that pass most of the selection requirements but fail one specific requirement. The fake ratio will be estimated using an entirely data based method in a sample disjoint from the candidate sample. The CHIso will be the separating requirement for jets in the fake ratio. Photons i.e. EM objects that have no track in the tracker, therefore, need to be separated into categories based on which requirements they meet: one where the photons pass all the selection requirements, and one where the photons pass all the selection requirements but the CHIso cuts. The sample of photons that pass all the requirements will be enriched with real photons and jets misidentified as photons. Then, the real photons in that sample will be removed so the fake ratio can be estimated as the number of events in the resulting sample over the number of events in the sample where the photons pass all the selection requirements but the CHIso cuts

Explicitly, there are three categories of photons are: *bad* photons, *mostly good - failed* photons, and *mostly good - passed* photons. *Mostly good* selection requirements are as follows:

For the barrel:

- $p_T > 15$ GeV,

- H/E < .105,

- NeuIso < 9.188 + .0126 * p_T + .000026 * p_T^2,

- PhoIso < 2.956 + .0035 * p_T.

For the endcap:

- p_T > 15 GeV,

- H/E < .029,

- NeuIso < 10.471 + .0119 * p_T + .000025 * p_T^2,

- PhoIso < 4.895 + .004 * p_T.

A *bad* photon fails the *mostly good* selection requirements. *Mostly good - passed* photons pass the *mostly good* selection requirements, and also pass a CHIso cut of CHIso < 2.839 in the barrel and CHIso < 2.150 in the endcap. *Mostly good - failed* photons pass the *mostly good* selection requirements, but fail the CHIso cut (Table 2). *Bad* photons will mainly consist of jets. *Mostly - good failed* photons will also mostly consist of jets. *Mostly - good passed* photons will consist of true photons and jets misidentified as photons.

Now, we define a control region that is dominated by $Z + \gamma + j$ where the γ is a photon and j is a jet. Specifically, the γ is from final state radiation. Events in this region are required to have two medium muons, one

Bad Photon	Mostly - Good Passed Photon	Mostly - Good Failed Photon
Fails *mostly good* requirements	Passes *mostly good* requirements In barrel: CHIso < 2.839 In endcap: CHIso < 2.150	Passes *mostly good* requirements In barrel: CHIso > 2.839 In endcap: CHIso > 2.150

Table 2: Summary of the selection requirements for different categories of photons.

photon is required to be a *mostly - good passed* photon, and the other photon is required to be a *mostly - good failed* photon. This control region will be used to create a template of the shower shapes of photons and jets in the barrel and endcap.

The control region is enriched with this type of events by making kinematic cuts on the data. Specifically, the invariant mass of the muons resulting from the Z boson is required to be between 50 GeV and 80 GeV. Furthermore, the invariant mass of the muons plus the photon is required to be between 60 GeV and 130 GeV.

Since this invariant mass is not merely a Gaussian centered around 91 GeV (Figure 5), a sideband subtraction must be preformed. So, a control sample where both photons are bad is created in order to model the continuum distribution of the background that is beneath the Gaussian. This sample is enriched with $Z + j + j$ events i.e. both of the photons are required to be *mostly - good failed*. This continuum distribution is then fitted to a functional form. A Landau was found to fit the distribution well (Fig. 6).
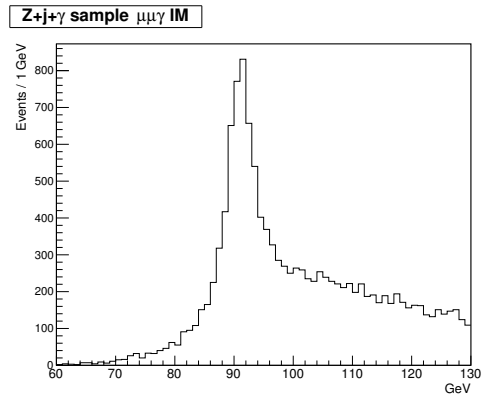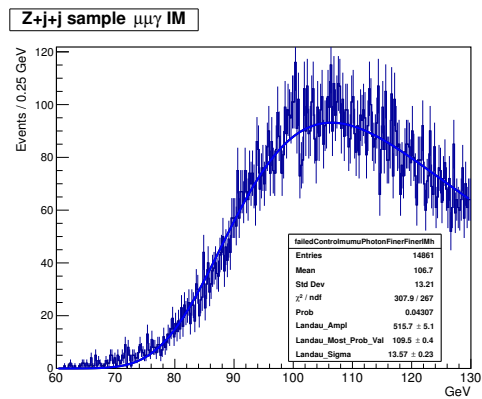
Figure 5: Unfitted Invariant mass

Figure 6: $Z + j + j$ control region fit with a Landau

With this information, the control region enriched with $Z + \gamma + j$
can be fitted with the functional form of a Gaussian on top of a Landau,
where the Gaussian represents signal events and the Landau represents
background events. Since photons are selected by different requirements
in the barrel and endcap and the shower shape distribution of photons is
different in the barrel and endcap, the control region is further divided into

23

two sub-regions: one where the photon was found in the barrel (Fig. 7), and the other where the photon was found in the endcap (Fig. 8).

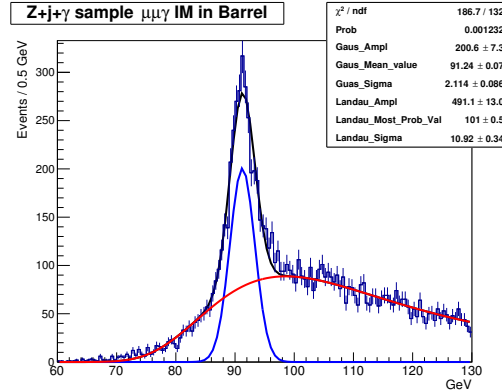Figure 7: $Z + j + \gamma$ control region where γ is in the barrel fit with a Gaussian + Landau
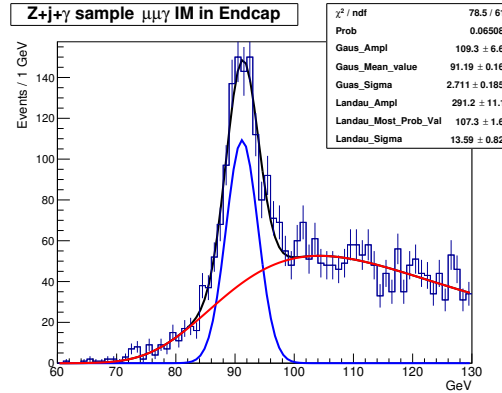

Figure 8: $Z+j + \gamma$ control region where γ is in the endcap fit with a Gaussian + Landau

By integrating the functional forms around the mass peak (within two standard deviations of the fitted Gaussian), an estimate of the number of signal and background events can be made. By integrating the Gaus-

sian, the estimate of the number of signal events was found to be 1057.85 in the barrel and 669.20 in the endcap. By integrating the Landau, the estimate of the number of background events was found to be 897.50 in the barrel and 355.17 in the endcap.

Since the distribution from an EM shower is much different than that of a hadronic shower, the shower shape of a photon is different than that of a jet. The shower shape distribution of *mostly - good failed* photons is a template of the shower shape of a jet. If the jets misidentified as photons were removed from the sample, then the *mostly - good passed* photons would be a template of the shower shape of a true photon. So, the shower shapes of the the *mostly good - failed* sample is scaled using the estimates for the number of background in the barrel and endcap. Then, these histograms are subtracted from the *mostly good - passed* sample's shower shape. This yields templates for the shower shapes of photons and jets in the barrel and endcaps (Figs. 9 - 12).
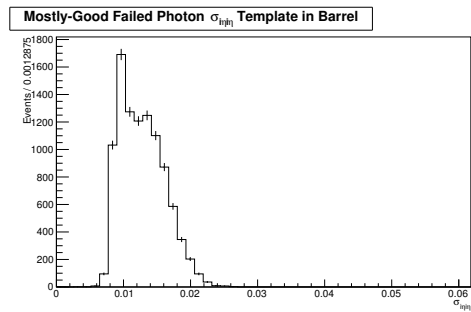

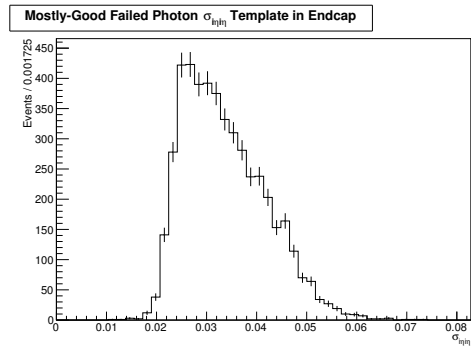Figure 9: Template of jet shower shape in barrel

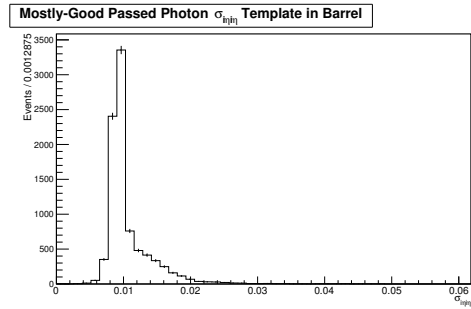Figure 10: Template of jet shower shape in endcap
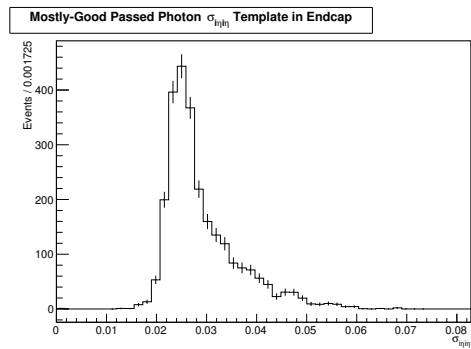

Figure 11: Template of Photon shower shape in barrel

Figure 12: Template of Photon shower shape in endcap

Now that the templates have been found, a new sample is made with-

26

out the restrictions on invariant mass with requirement that the event has one *bad* photon while the other photon can either be a *mostly - good failed* or a *mostly - good passed* photon. This sample will be composed of both $Z + \gamma + j$ and $Z + j + j$. The requisite *bad* photon ensures that this sample is independent of the candidate sample. The shower shape plots for this sample are in Figures 13 to 16.
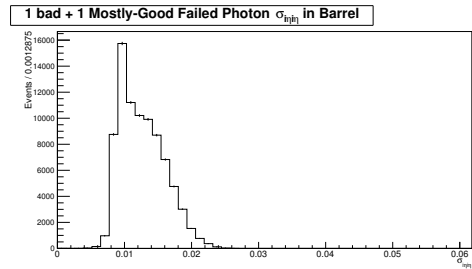

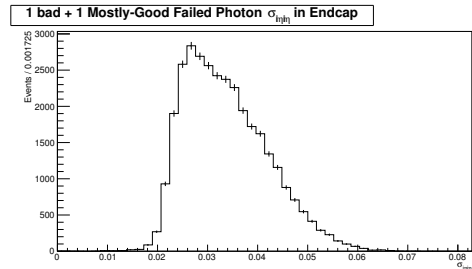Figure 13: Jet shower shape in barrel without kinematic cuts

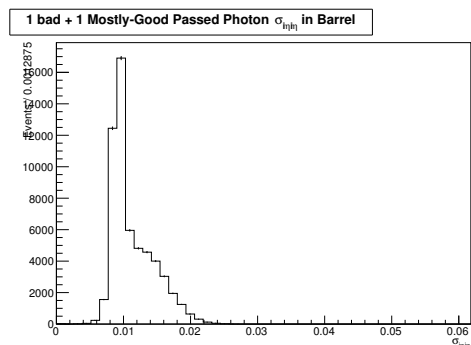Figure 14: Jet shower shape in endcap without kinematic cuts

Figure 15: Photon shower shape in barrel without kinematic cuts
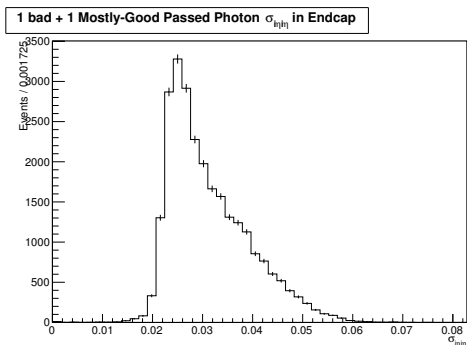
Figure 16: Photon shower shape in endcap without kinematic cuts

The templates for the jet and photon shower shapes can be used to fit the shower shapes of the photons in the sample without the kinematic cuts to determine how many of the events had photons in the final state and how many actually had jets misidentified as photons. It was found that 0.598 ± 0.011 of the shower shape of the one *bad* + one *mostly good - passed* sample in the barrel can be accounted for by the *mostly good - passed* template. 0.402 ± 0.010 of the shower shape was accounted for by the *mostly good -failed* template. Similarly, it was found that 0.489 ± 0.022

of the shower shape of the one *bad* + one *mostly good - passed* sample in the endcap can be accounted for by the *mostly good - passed* template. 0.511 ± 0.021 of the shower shape was accounted for by the *mostly good -failed* template (Table 3).

	Barrel Fraction	Endcap Fraction
Mostly Good - Passed Template	0.598 ± 0.011	0.489 ± 0.022
Mostly Good - Failed Template	0.402 ± 0.010	0.511 ± 0.021

Table 3: Fraction of the photon shower shapes in the sample without kinematic cuts that can be accounted for by the *mostly good - passed* and *mostly good - failed* templates in the barrel and endcap.

The templates are then added to each other weighted by the fraction that they make up the fitted template multiplied by the number of events in the fitted template. The resulting histogram is compared to the fitted histogram (Fig. 17 and Fig. 18) using the χ^2-Test. The probability that the weighted addition of the template histograms and the fitted histogram in the barrel came from the same distribution is approximately 1. The probability that the weighted addition of the template histograms and the fitted histogram in the endcap came from the same distribution is approximately 1.
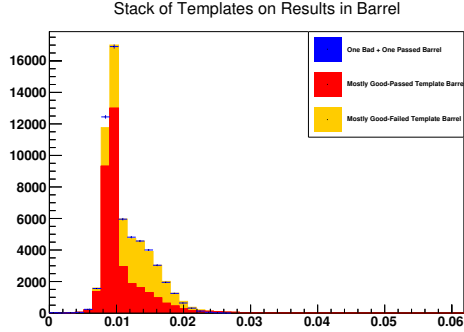
Figure 17: Stack of the weighted templates superimposed on the histogram that the templates were fitted to in the barrel.
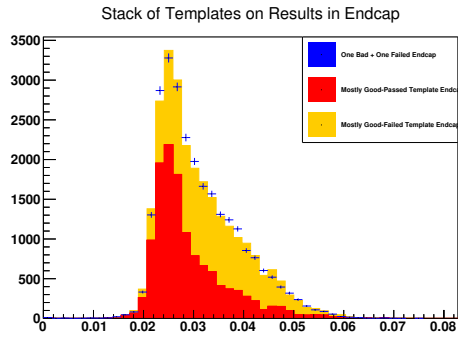

Figure 18: Stack of the weighted the templates superimposed on the histogram that the templates were fitted to in the endcap.

Now, with the scaled templates, the fake ratio can be found by integrating the *mostly - good failed* template from zero to the $\sigma_{i\eta i\eta}$ cut given by the loose photon selection requirements and dividing this integral by the number of events in the $Z + j + j$ sample, where one jet is a *bad* photon and the other jet is a *mostly - good failed* photon. The fake ratio was found to be 0.081 ±0.005 in the barrel and 0.115 ±0.012 in the endcap (Table 4).

30

	Integral of Scaled Mostly-Good Failed Template	Number of events in One Bad + One Failed Sample	Fake Ratio
Barrel	6708.82 ± 430.09	83113 ± 288.29	0.081 ±0.005
Endcap	3714.81 ± 373.79	32233 ± 179.54	0.115 ±0.012

Table 4: Fake Ratio estimation for barrel and endcap

5   Results

The probability that a true photon will pass *mostly-good passed* selection requirements is given by the photon efficiency. Photon efficiency (ϵ) is the ratio of the number of photons selected by selection requirements over the number of all the real photons in the sample. The loose photon selection requirements have been tuned by the CMS collaboration so that the photon efficiency is 0.9. The probability that a jet will pass *mostly-good passed* selection requirements is given by the fake ratio. Multiplying the number of photons by the photon efficiency yields the number of those events that will pass *mostly-good passed* selection requirements. Multiplying the number of photons by the complement of the photon efficiency yields the number of those events that will pass *mostly-good failed* selection requirements. This is similarly true for jets and the fake ratio. Treating each of the EM objects in the final state as independent, the number of events with final states of *mostly-good passed* + *mostly-good passed*, *mostly-good passed* + *mostly-good failed*, *mostly-good failed* + *mostly-good passed*, and *mostly-good failed* + *mostly-good failed* can be estimated by multiplying the number of events with the final states of $\gamma + \gamma$, $\gamma + j$, $j + \gamma$, and $j + j$ by the appropriate factor and summing the results. This is summarized in the following matrix equation [8]:

$$
\begin{pmatrix} N_{pp}^{\gamma\gamma} \\ N_{pf}^{\gamma\gamma} \\ N_{fp}^{\gamma\gamma} \\ N_{ff}^{\gamma\gamma} \end{pmatrix} = \begin{pmatrix} \epsilon_1\epsilon_2 & \epsilon_1 f_2 & \epsilon_2 f_1 & f_1 f_2 \\ \epsilon_1(1-\epsilon_2) & \epsilon_1(1-f_2) & (1-\epsilon_2)f_1 & f_1(1-f_2) \\ (1-\epsilon_1)\epsilon_2 & (1-\epsilon_1)f_2 & \epsilon_2(1-f_1) & (1-f_1)f_2 \\ (1-\epsilon_1)(1-\epsilon_2) & (1-\epsilon_1)(1-f_2) & (1-\epsilon_2)(1-f_1) & (1-f_1)(1-f_2) \end{pmatrix} \begin{pmatrix} N_{\gamma\gamma} \\ N_{\gamma j} \\ N_{j\gamma} \\ N_{jj} \end{pmatrix}
$$

$$(3)$$

where the subscript of 1 refers to the leading EM object and 2 refers to the trailing EM object. N refers to the proportion of events that are in the category. The entries of each vector sum to 1. The left subscript refers to the leading EM object and the right subscript refers to the trailing EM object. The subscript p denotes an EM object that falls into the *mostly - good passed* category and the subscript f denotes an EM object that falls into the *mostly - good failed* category. The subscript γ denotes an EM object that is a photon, and the subscript j denotes an EM object that is a jet.

The matrix can be inverted so that knowing the number of events for each combination of EM objects that pass or fail the mostly good selection requirement yields the number of events where the EM objects are $\gamma\gamma$, γj, $j\gamma$, and jj. Inverting the matrix gives the following equation:

$$
\begin{pmatrix} N_{\gamma\gamma} \\ N_{\gamma j} \\ N_{j\gamma} \\ N_{jj} \end{pmatrix} = \frac{1}{[\epsilon_2(1-f_2)-f_2(1-\epsilon_2)][\epsilon_1(1-f_1)-f_1(1-\epsilon_1]} \begin{pmatrix} (1-f_2)(1-f_1) & -f_2(1-f_1) & -(1-f_2)f_1 & f_1f_2 \\ -(1-\epsilon_2)(1-f_1) & \epsilon_2(1-f_1) & f_1(1-\epsilon_2) & -\epsilon_2 f_1 \\ -(1-\epsilon_1)(1-f_2) & (1-\epsilon_1)f_2 & \epsilon_1(1-f_2) & -\epsilon_1 f_2 \\ (1-\epsilon_1)(1-\epsilon_2) & -(1-\epsilon_1)\epsilon_2 & -\epsilon_1(1-\epsilon_2) & \epsilon_1\epsilon_2 \end{pmatrix} \begin{pmatrix} N_{pp}^{\gamma\gamma} \\ N_{pf}^{\gamma\gamma} \\ N_{fp}^{\gamma\gamma} \\ N_{ff}^{\gamma\gamma} \end{pmatrix}
$$
(4)

Both ϵ_1 and ϵ_2 are 0.9 since loose photon selection requirements were used. $N_{pp}^{\gamma\gamma}$, $N_{pf}^{\gamma\gamma}$, $N_{fp}^{\gamma\gamma}$, and $N_{ff}^{\gamma\gamma}$ come directly from the data (Table 5).

	$N_{pp}^{\gamma\gamma}$	$N_{pf}^{\gamma\gamma}$	$N_{fp}^{\gamma\gamma}$	$N_{ff}^{\gamma\gamma}$
BB	1382 ± 37	733 ± 27	687 ± 26	681 ± 26
BE	395 ± 20	208 ± 14	213 ± 215	208 ± 14
EB	398 ± 20	231 ± 15	235 ± 15	280 ± 17
EE	151 ± 12	72 ± 8	73 ± 9	82 ± 9

Table 5: Number for each Mostly Good - Passed/Mostly Good-Failed combination.

With the measured fake ratios (Table 4), Equation 4 can now be evaluated for the four detector region combinations. The resulting vector yields the proportion of events for each final state. This vector is then multiplied by the number of candidate events for each region in order to estimate the number of events in each final state (Table 6).

	$N_{\gamma\gamma}$	$N_{\gamma j}$	$N_{j\gamma}$	N_{jj}
BB	630.72 ± 46.99	257.43 ± 33.88	235.15 ± 32.83	258.7 ± 87.92
BE	171.57 ± 25.31	73.43 ± 18.85	69.29 ± 18.43	80.72 ± 49.77
EB	154.17 ± 25.42	66.23 ± 19.22	75.41 ± 20.02	102.19 ± 52.61
EE	67.79 ± 15.75	23.55 ± 11.22	24.06 ± 11.29	35.60 ± 31.57

Table 6: Estimation of number of events in each final state.

The estimated number of $\mu\mu\gamma\gamma$ events is the sum of N$_{\gamma\gamma}$ events in all the detector regions. (Table 7). The total number of $\mu\mu\gamma\gamma$ events is 1024.25 ± 61.18 events. The production of $Z\gamma\gamma$ events at next-to-leading order generated by MADGRAPH5.aMC@NLO has an estimated cross section of 5.01 ± 1.09 fb in the muon channel. Multiplying the cross section by the integrated luminosity for Run 2 gives the Standard Model's prediction for the number of $Z\gamma\gamma$ events produced in Run 2. The Standard Model predicts 681.86 ± 148.17 events, so there seems to be an excess number of observed $Z\gamma\gamma$ events over the Standard Model prediction.

	$N_{pp}^{\gamma\gamma}$	$N_{\gamma j}+N_{j\gamma}+$ N_{jj}	$N_{\gamma\gamma}$
BB	1382 ± 37	751.28 ± 99.77	630.72 ± 46.99
BE	395 ± 20	223.44 ± 56.32	171.57 ± 25.31
EB	398 ± 20	243.83 ± 59.48	154.17 ± 25.42
EE	151 ± 12	83.21 ± 35.36	67.79 ± 15.75
Total	2326 ± 48	1301.75 ± 133.85	1024.25 ± 61.18

Table 7: The number of candidate events followed by the number of background and signal events

6   Conclusion

The purpose of this analysis was to estimate the number of $Z\gamma\gamma$ events produced during Run 2 at CMS through the muon channel. The total number of background events was estimated to be 1319.76 $\pm$ 133.84, and the number of $Z\gamma\gamma$ events where the Z boson decayed to muons was found to be 1024.25 $\pm$ 61.18 which seems to be an excess over the Standard Model's prediction of 681.86 $\pm$ 148.17 events. This was achieved by first selecting a candidate sample and then subtracting the estimate number of background events. The number of background events was estimated by calculating the fake ratio, which was found to be 0.081 $\pm$0.005 in the barrel, and 0.115 $\pm$0.012 in the endcap, and using that in the matrix equation (Equation 4).

7   Appendix

7.1   Medium Muon Selection Requirements

A medium muon is a event that identified as a muon by the Particle-Flow [7] event reconstruction, and is also reconstructed as a global-muon or as an arbitrated tracker-muon. 80% of the muon candidate's tracker hits must be valid, and the muon candidate must also satisfy either of the following sets of requirements:

- The muon candidate is a global muon.

- The muon candidate's normalized global-track has a $\chi^2 < 3$.

- The muon candidate's Tracker and Standalone position match i.e. their $\chi^2 < 12$.

- The muon candidate's kick finder < 20.

- The muon candidate has a segment compatibility > 0.303.

  or

- The muon candidate has a segment compatibility > 0.451.

7.2 Candidate Sample's Qualities

Figures 19 to 30 display the ϕ, η, and p_T distribution of each object in the events in the N_{pp} category.
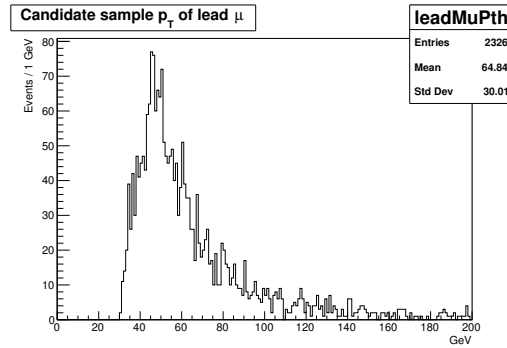
Figure 19: p_T distribution of the lead muon in the candidate sample.
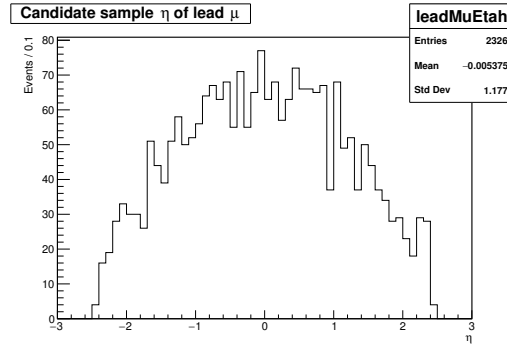
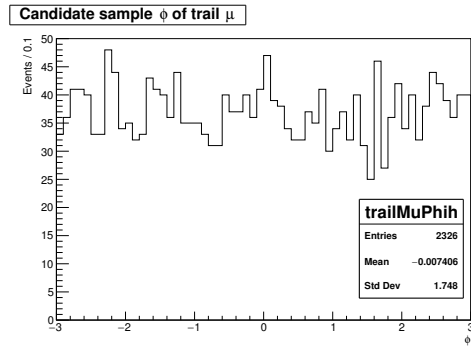Figure 20: η distribution of the lead muon in the candidate sample.
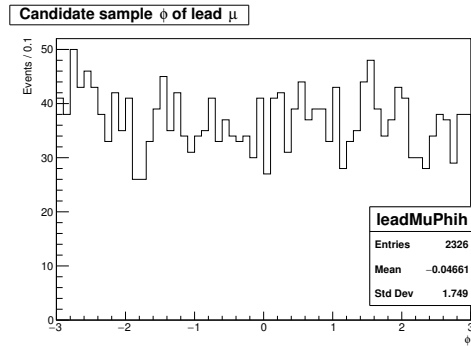
Figure 21: ϕ distribution of the lead muon in the candidate sample.
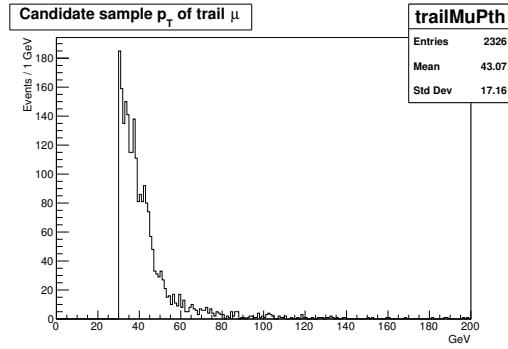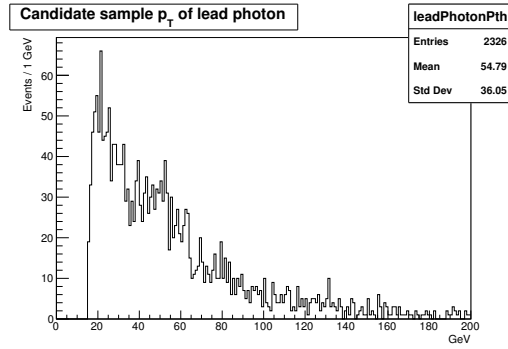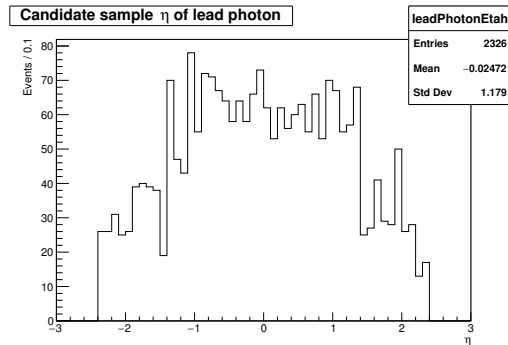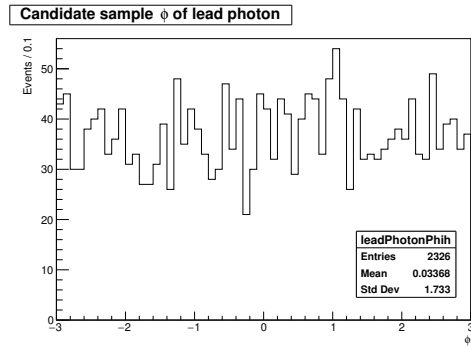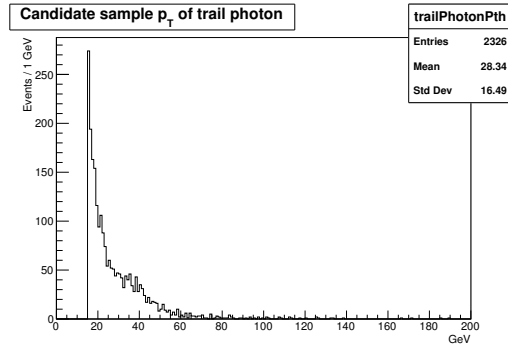

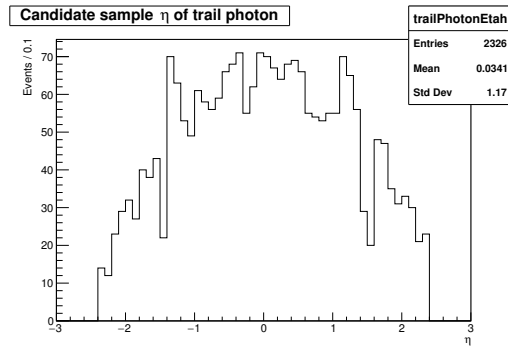Figure 22: p_T distribution of the trail muon in the candidate sample.
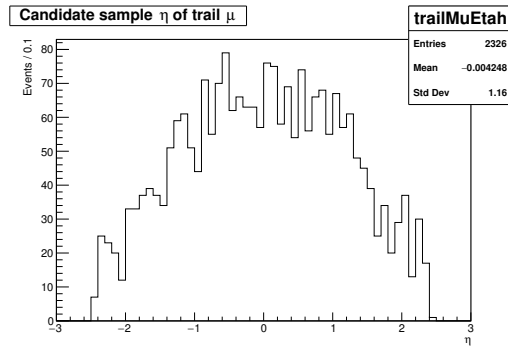
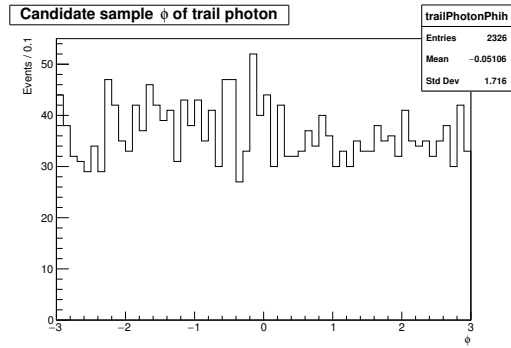Figure 23: η distribution of the trail muon in the candidate sample.

40

Figure 24: ϕ distribution of the trail muon in the candidate sample.

Figure 25: p_T distribution of the lead photon in the candidate sample.

Figure 26: η distribution of the lead photon in the candidate sample.

41

Figure 27: ϕ distribution of the lead photon in the candidate sample.

Figure 28: p_T distribution of the trail photon in the candidate sample.

Figure 29: η distribution of the trail photon in the candidate sample.

42

Figure 30: ϕ distribution of trail photon in the candidate sample.

7.3   Background Sample's Qualities

Figures 31 to 36 display the ϕ, η, and p_T distribution of the photons in the N_{pf}, N_{fp}, and N_{ff} categories added together.
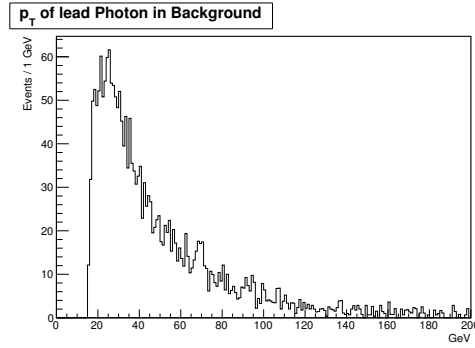

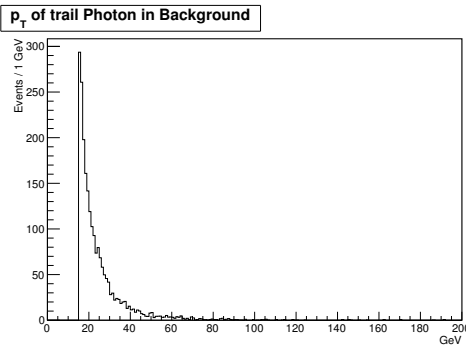Figure 31: p_T distribution of the leading photons in the background sample.

Figure 32: p_T distribution of the trailing photons in the background sample.
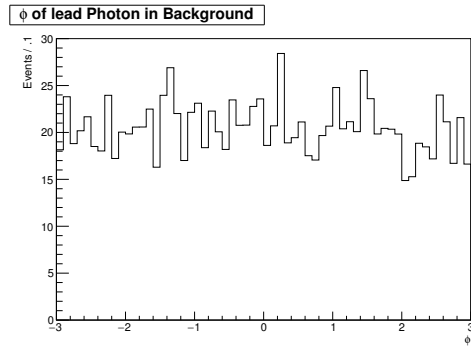
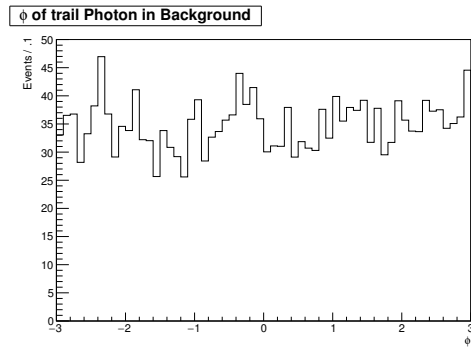Figure 33: ϕ distribution of the lead photons in the background sample.

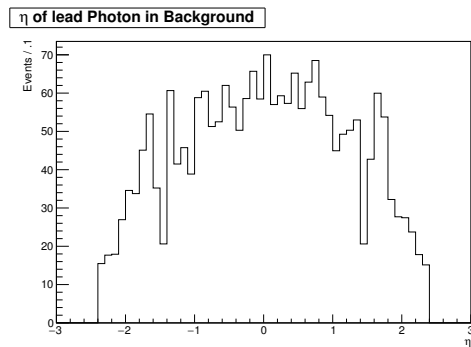Figure 34: ϕ distribution of the trail photons in the background sample.

Figure 35: η distribution of the lead photons in the background sample.
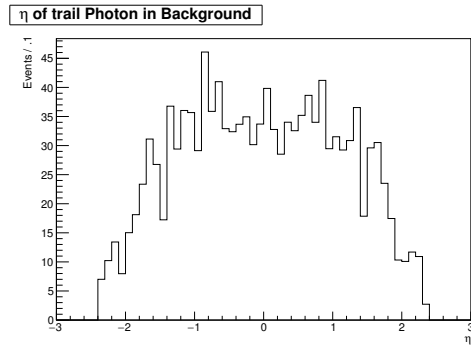
Figure 36: η distribution of the trail photons in the background sample.

References

[1] University of Notre Dame, "Standard Model
of Fundamental Particles and Interations",
https://www3.nd.edu/ cjessop/research/overview/particle_chart.pdf

[2] The ATLAS Collaboration, "Measurements of $Z\gamma$ and $Z\gamma\gamma$ production in pp collisions at $\sqrt{s} = 8$ TeV with the ATLAS detector", *Phys. Rev. D 93, 112002* (2016).

[3] The CMS Collaboration, "Tracking.", *Tracking CMS Experiment*,
http://cms.cern/detector/identifying-tracks.

[4] The CMS Collaboration, "Energy of Electrons and Photons
(ECAL).", *Energy of Electrons and Photons (ECAL) CMS Experiment*, http://cms.cern/detector/measuring-energy/energy-electrons-and-photons-ecal.

[5] "Hadron Calorimeter: CMS Experiment." *Hadron Calorimeter — CMS Experiment*, cms.web.cern.ch/news/hadron-calorimeter.

[6] The CMS Collaboration, "Detecting Muons.", *Detecting Muons CMS Experiment*, http://cms.cern/detector/detecting-muons.

[7] Andrew Askew. "ECAL Clustering".
www.hep.fsu.edu/ askew/wbpge/Askew_PhotonHATS_Clustering.pdf

[8] Sirunyan, A. M. et al. "Measurements of the pp $\to$ W$\gamma\gamma$ and pp $\to$ $Z\gamma\gamma$ Cross Sections and Limits on Anomalous Quartic Gauge Couplings at $\sqrt{s}$ = 8 TeV." *Journal of High Energy Physics 2017.10* (2017)

[9] The L3 Collaboration, "Measurement of the $e^+e^- \to Z\gamma\gamma$ Cross Section and Determination of Quartic Gauge Boson Couplings at LEP", *Phys.Lett.B478:39-49* (2000).